Jerome

Environment Canada
Environnement Canada

National Water Research Institute
Institut National de Recherche sur les Eaux

Environmental Spectro-Optics Section

National Water Research Institute

Canada Centre for Inland Waters

Burlington, Ontario

Inland Waters Direction Générale

EFFECT OF SOLAR ZENITH ANGLE DIURNAL VARIATIONS ON ESTIMATIONS OF PRIMARY PRODUCTION AND IRRADIATION

by

J.H. Jerome, R.P. Bukata, and J.E. Bruton

Environmental-Spectro-Optics Section

National Water Research Institute

Canada Centre for Inland Waters

Burlington, Ontario

Running Head: SOLAR ANGLE AND IRRADIATION

ABSTRACT

Monte Carlo simulations of the propagation of photons through a variety of water types are utilized in conjunction with the Vollenweider-Fee primary production model to determine the effect of the diurnal variation of solar zenith angle on estimations of primary production and irradiation. Such effects are considered as a function of both geographic latitude (northern hemisphere) and time of year. It is shown that the effect of solar zenith angle dependence of subsurface irradiance levels on the determination of daily primary production is small ($< \pm 15\%$) for any latitude or time of year. The effect of solar zenith angle dependence on the determination of irradiation at a given depth, however, can be quite significant. Under certain conditions of latitude and time this effect can be as large as $\pm 80\%$.

INTRODUCTION

One of the most significant parameters governing the photosynthetic processes in natural water bodies is the daily integrated value of subsurface irradiance within the water column. Various models have been proposed for mathematically estimating primary production, among the most notable being those of Smith (1936), Talling (1957), Vollenweider (1965), and others reviewed in Vollenweider (1965) and Patten (1968). Fee (1969) has presented a numerical solution of the Vollenweider photosynthesis model which enables an exploitation of its full generality. In this paper we utilize the Fee numerical solution in conjunction with a realistic appraisal of the variability of subsurface irradiance levels to evaluate the effect of the diurnal variation of solar zenith angle on the accuracy to which daily integrated values of subsurface irradiance may be estimated.

The integrated value of subsurface irradiance is dependent upon not only the inherent optical properties (absorption and scattering) of the various components of the water mass and the nature of the incident solar and skylight radiance distributions, but also the solar zenith angle at the time of subsurface irradiance level determination. The diurnal variation of solar zenith angle is itself a function of Julian day and geographic latitude.

A detailed description of the propagation of radiation through natural water masses requires a consideration of both the angular distribution of the incident radiation field and the optical properties of the water. Those optical properties which influence radiative propagation are the total attenuation coefficient c (defined as the sum of the absorption coefficient a and the scattering coefficient b), the scattering albedo ω (defined as the ratio b/c and representing that proportion of photonic interactions in the water that are scattering events), and the backscattering probability B (the probability that a scattering interaction will result in a photon being scattered into the backward hemisphere). Recently we have shown (Jerome et al., 1982) that the scattering albedo ω has a much greater influence on the solar zenith angle dependence of subsurface irradiance levels than does the backscattering probability B. Basically, the lower the value of ω defining a natural water mass (i.e., the smaller the percentage of scattering interactions occurring within the water column), the more pronounced will be the solar zenith angle dependence.

INCIDENT RADIATION FIELD

The incident radiation field considered in this analysis was taken to be comprised of a direct incident beam superimposed upon an isotropic diffuse radiance distribution. Obviously, on any given day,

such an incident radiation distribution can display large variations, ranging from nearly totally direct to totally diffuse. The effects of such variations in incident radiation distributions on the depths of subsurface irradiance levels have been discussed elsewhere (Jerome et al., 1982). For the purpose of this work, we have considered an incident radiation field determined from the clear-day global radiation model of Davies et al., (1975). On the basis of this model, a direct solar irradiance E_{sun} and a diffuse sky irradiance E_{sky} were obtained from

$$E_{sun} = (E_{sol} \cos\theta_i)\ \phi_{WA}\ \phi_{DA}\ \phi_{WS}\ \phi_{RS}\ \phi_{DS}/R^2 \qquad (1)$$

$$E_{sky} = (E_{sol} \cos\theta_i)\ \phi_{WA}\ \phi_{DA}\ (1-\phi_{WS}\ \phi_{RS}\ \phi_{DS})/2R^2 \qquad (2)$$

where E_{sol} = solar irradiance at the mean annual earth-sun distance (i.e. at 1 Astronomical Unit)

θ_i = solar zenith angle (θ_i = 0 at sun directly overhead)

R = radius vector (expressed in Astronomical Units)

and ϕ_{WA}, ϕ_{DA}, ϕ_{WS}, ϕ_{RS} and ϕ_{DS} are atmospheric parameters which account for scattering and absorption effects of atmospheric water and dust, and Rayleigh scattering. These parameters are obtained from air mass and precipitable water content of the atmosphere in the manner described by Davies et al., (1975). Table 1 lists the incident radiation distribution (with the diffuse component

expressed as a percentage of incident radiation) as a function of solar zenith angle used in this analysis. Table 1 was constructed assuming a precipitable water content of 1.5 cm, a value which reasonably approximates the range of atmospheric conditions normally encountered. It should be emphasized that Table 1 represents a clear-day atmosphere.

Such an incident radiation distribution was considered impinging upon a planar horizontal water surface. For each incident angle θ_i, a refracted angle θ_r was calculated. Surface reflection of the direct solar beam was considered at each value of θ_i utilizing the angular dependency of the Fresnel reflectivities, and the direct solar beam was adjusted to incorporate the effects of the surface reflection. The diffuse sky radiation was corrected for surface reflection by subtracting 6.6% of its incident value at all times (Jerlov, 1976).

DETERMINATION OF SUBSURFACE IRRADIANCE LEVELS

Figure 1 schematically illustrates in ray form the path of an incident beam (solar zenith angle θ_i, refracted angle θ_r) entering the water surface. $Z_L(\theta_r)$ is the path length along the principal direction of subsurface propagation to a particular irradiance level. Z is the vertical distance to that level.

The most generally used expression for the attenuation of subsurface irradiance is Beer's Law, which may be expressed as

$$E(Z,\theta_r) = E_o(\theta_r)\exp(-kZ_L(\theta_r)) \tag{3}$$

where $E(Z,\theta_r)$ = irradiance at depth Z

$E_o(\theta_r)$ = irradiance just beneath the surface

k = irradiance attenuation coefficient

Replacing Z_L by the vertical depth Z in equation (3) yields

$$E(Z,\theta_r) = E_o(\theta_r)\exp(-k_v Z) \tag{4}$$

where k_v is the vertical attenuation coefficient.

Since $Z = Z_L$ only for the condition of the sun directly overhead (i.e., $\theta_i = \theta_r = 0$), the value of k_v varies with the time at which the subsurface measurements were performed. Extending the use of an invariant k_v throughout the daylight hours, therefore, clearly neglects the inappropriateness of equation (4) for non-zero values of θ_r. Such a diurnal variation was taken into account by establishing a Monte Carlo program which simulated the propagation of photons incident upon a variety of water types from a spectrum of θ_i values.

In such a Monte Carlo simulation a water type is chosen (by selecting a value of ω and B) and individual photons are traced through the water medium following each absorption or scattering interaction in a sequential manner. After a sufficient number of photons are traced to provide small statistical errors, the results are appropriately summed to obtain the depths of the desired irradiance levels.

Three different water types are considered, characterized by $\omega = 0.60$, $\omega = 0.75$, and $\omega = 0.90$, respectively, each of the three water types displaying progressively higher percentages of scattering interactions. A value of B = 0.0285 was selected, this value being an average value appropriate to two scattering phase functions taken from Petzold (1972). Since the scattering albedo ω has a much greater effect on the diurnal zenith angle dependence of subsurface irradiance levels than does the backscattering probability B (Jerome et al., 1982), the value of B selected in this study would not detract significantly from the generality of application of these results to most natural water bodies.

Two separate incident radiation distributions are considered as inputs to the Monte Carlo program, a direct beam at incident angle θ_i and an isotropic diffuse radiance distribution.

For the direct incident beam, the results of the Monte Carlo simulation were curve fitted to Beer's Law of equation (3) which was rewritten as a series expansion in $\cos\theta_r$ of the form

$$E(Z,\theta_r) = E_o(\theta_r) \exp\left[-kZ/\sum_{i=1}^{3} r_i(\omega)\cdot(\cos\theta_r)^i\right] \qquad (5)$$

where $r_i(\omega)$ are series expansion coefficients, a different set of such coefficients being appropriate to each subsurface irradiance level. Table 2 lists the values of $r_i(\omega)$ as determined for the direct component of the incident radiation for the three values of ω considered in this work and for the 30%, 10%, 3%, and 1% irradiance levels.

For the diffuse incident radiation distribution, no solar zenith angle dependence is possible. For a purely diffuse incident radiation field, equation (5) reduces to

$$E(Z) = E_o \exp\left[-kZ/r\right] \qquad (6)$$

As a consequence, only one value of r is obtained for each irradiance level. These values of r for a diffuse incident radiation distribution are also listed in Table 2.

Figures 2(a) and 2(b) illustrate the relative depth of the 30%, 10%, 3%, and 1% subsurface irradiance levels as a function of solar zenith angle (0° solar zenith angle indicates the sun directly overhead) obtained from the Monte Carlo simulations for water masses of $\omega = 0.60$ and $\omega = 0.90$ respectively. It is clearly seen that:

a) A distinct solar zenith angle dependence is exhibited by the subsurface irradiance levels.

b) The solar zenith angle dependence increases with decreasing level of irradiance.

c) The solar zenith angle dependence decreases with increasing ω.

In the generation of Figure 2, the input radiation distribution for the clear day atmosphere of Table 1 was utilized in the Monte Carlo simulation as follows:

a) For a given irradiance level X% and two values of solar zenith angle θ and 0, equation (5) for a direct incident beam yields:

$$\ln \left[\frac{E_x(0)}{E_x(\theta)}\right] = k \left[\frac{Z_x(\theta)}{f(\theta)} - Z_x(0)\right] \qquad (7)$$

where $Z_X(\theta)$ = depth of the X% irradiance level at solar zenith angle θ

$Z_X(0)$ = depth of the X% irradiance level at solar zenith angle 0

and $f(\theta) = \sum_{i=1}^{3} r_i(\omega,X) \cdot (\cos\theta_r)^i$

Since $E_X(0) = E_X(\theta)$,

$$Z_X(\theta) = Z_X(0)\ f(\theta) \tag{8}$$

for each irradiance level.

b) Similarly, for a given irradiance level X% and two values of solar zenith angle θ and 0, equation (6) for an isotropic incident radiance distribution yields:

$$Z'_X(\theta) = Z'_X(0) \tag{9}$$

where the primed values of Z_X refer to depths arising from an incident radiation field that is totally diffuse.

c) The resultant depth of a given irradiance level X% for an input radiation distribution comprised of both direct and diffuse components may be written as

$$Z_X(\theta) = F\ Z'_X(0) + (1-F)\ f(\theta)\ Z_X(0) \tag{10}$$

where F is the fraction of the incident radiation just below the surface that is diffuse and the other terms are as defined in equations (8) and (9).

For a given value of k, the Monte Carlo simulation will determine values of $Z_x(0)$ and $Z'_x(0)$. For illustrative purposes, k was set at 1.0 in the generation of Figure 2.

DETERMINATION OF PRIMARY PRODUCTION

The Fee (1969) integration of the Vollenweider (1965) primary production model is expressed as

$$\sum_t \sum_Z P = P_{opt}\, \delta \int_{\frac{-\lambda}{2}}^{\frac{\lambda}{2}} \int_{0.01\frac{E_o}{E_k}(t)}^{\frac{E_o}{E_k}(t)} \frac{dydt}{k_v(t)\left[\left(1+y^2\right)\left(1+(ay)^2\right)^n\right]^{0.5}} \qquad (11)$$

where P = rate of photosynthesis per unit area of surface per day

a,n = parameters of the model

P_{opt} = optimum rate of photosynthesis per unit volume of water

$\delta = P_{max}/P_{opt}$ where P_{max} is the maximum rate of photosynthesis per unit volume when a or n = 0

$E_o(t)$ = irradiance just below the surface at time t

$y = E_o(t)/E_k$ where E_k is the light saturation parameter when a or n = 0

λ = day length

$k_v(t)$ = vertical attenuation coefficient

In the Fee integration of the Vollenweider model, the vertical attenuation coefficient k_v was considered to be a constant determined from applying Beer's Law to an irradiance profile. However, as seen from Figure 1, k_v displays a solar zenith angle dependence, and is therefore a function of time. The limits of integration in equation (11) are the times of local sunrise and local sunset, and the values of y corresponding to the surface and the depth of the 1% irradiance level, below which depth no significant contribution to primary production is considered to occur.

The steps taken in arriving at a value of the daily primary production within a water column bounded by the surface and the 1% irradiance level were:

a) From the atmospheric model, the direct and diffuse incident irradiance values were determined as a function of time from sunrise to sunset.

b) These incident irradiance values were taken through the air/water interface correcting for surface reflection to obtain values of $E_o(t)$ for each of the direct and diffuse subsurface incident components.

c) For a given value of k, the Monte Carlo simulation was used to determine values of $Z_x(0)$ and $Z'_x(0)$ for the 30%, 10%, 3%, and 1% irradiance levels. Utilizing these values of $Z_x(0)$ and $Z'_x(0)$ in conjunction with the $r_i(\omega)$ values listed in Table 2, equation (10) was then used to determine the depth $Z_x(\theta)$ of each irradiance level throughout the day.

d) Using the values of $Z_x(\theta)$ obtained for each of the above four subsurface irradiance levels (plus the surficial 100% irradiance level), a 5-point least-squares fit readily determined the required $k_v(t)$ values. That is, the time dependent $k_v(t)$ was obtained throughout the day. The θ_i dependence (i.e., the time-related

dependence) of $k_v(t)$ is illustrated in Figure 3. Two features are evident from Figure 3: (i) As ω increases the θ_i dependence of $k_v(t)$ decreases; (ii) the relative value of $k_v(t)$ (for all values of ω) increases with increasing solar angles up to ~70° at which point the relative value of $k_v(t)$ decreases. This decrease in the relative value of $k_v(t)$ at large solar zenith angles is due to the rapidly increasing percentage of diffuse radiation in the total incident radiation observed for large solar zenith angles.

e) In the original Fee expression k_v was considered a constant and could be taken outside the integral sign. This is equivalent to considering that the depth of the X% irradiance level is invariant in time (or θ). To obtain a constant k_v for this analysis we assumed an irradiance profile was taken at a particular solar zenith angle θ_i. We further assumed that this value would be appropriate for the entire solar day. As seen from Figure 3 this is clearly not the case, particularly for solar zenith angles $>$~30°. In the current expression of the Fee analysis (equation (11)), the solar angle dependence of k_v is considered.

Both forms of the integration were solved and the difference between the resulting values of $\Sigma\Sigma P$ (hereafter referred to as the inaccuracy in the determination of primary production by neglecting the solar angle dependence of subsurface irradiance levels) was calculated as

$$\% \text{ Inaccuracy} = \left[\frac{\Sigma\Sigma P_F - \Sigma\Sigma P}{\Sigma\Sigma P}\right] \cdot 100\% \qquad (12)$$

where $\Sigma\Sigma P_F$ refers to equation (11) with k_v = constant.

Half-hour averages of subsurface $E_o(t)$ were determined from sunrise to sunset for both the direct and diffuse components of incident radiation. To obtain a k_v, values of $k_v(t)$ were determined for each 10° of solar zenith angle. These values of $k_v(t)$ were then taken to correspond to the fixed value of k_v that would be assumed throughout the day if measurements were taken at that solar zenith angle. $k_v(t)$ was expressed as half-hour averages from sunrise to sunset. Whereas the half-hour averages of $E_o(t)$ were utilized in determining both $\Sigma\Sigma P$ and $\Sigma\Sigma P_F$, the fixed values of k_v were utilized in the determination of $\Sigma\Sigma P_F$ while the half-hour averages of $k_v(t)$ were utilized in the determination of $\Sigma\Sigma P$. The selection of a particular constant

value of k_v (dependent upon the time of day a measurement is performed) determines the % inaccuracy in the estimation of primary production.

f) The above analyses were repeated for three water types ($\omega = 0.60$, $\omega = 0.75$, and $\omega = 0.90$), four times of year (vernal and autumnal equinoxes (March and September) and summer and winter solstices (June and December)) and nine latitudes (10° intervals from 0° to 80°N). Various values of the Vollenweider model parameters a, n, P_{opt} and E_k and the irradiance attenuation coefficient k of equation (7) were also considered.

DISCUSSION I

The use of equation (12) in determining the percent inaccuracy in the determination of primary production was completely independent of the selection of a, n, P_{opt}, E_k and k. It was, however, very dependent upon the selection of ω, time of year, latitude and time of day (i.e., solar zenith angle θ_i) at which k_v was determined.

Table 3 lists the % inaccuracies determined from equation (12) for latitudes of 0°, 30°N, and 60°N for each of the

three water types (ω = 0.60, 0.75, and 0.90) and for the four times of year (March, September, June and December) as a function of solar zenith angle at the time of k_v determination. The % inaccuracies observed at the equinoxes (March and September) were invariably identical. Table 3 illustrates that both overestimates (indicated by positive entries) and underestimates (indicated by negative entries) of the primary production are possible in an anticipated manner. Measurements performed with the sun nearly vertically overhead (i.e., small values of θ_i) will be characterized by the largest overestimates of primary production while measurements performed with a rising or setting sun (i.e., large values of θ_i) will be characterized by the largest underestimates of primary production. This is a consequence (see Figure 3) of the determined k_v being respectively an underestimate and an overestimate of the average of $k_v(t)$ for the entire day. Clearly, therefore, there exists some intermediate value of θ_i at which the determined k_v is an appropriate estimate of the average value of $k_v(t)$ for the entire day, i.e., a value of θ_i exists for which the % inaccuracy will be zero. If a single irradiance profile were used to determine k_v this value of θ_i would be the obvious solar zenith angle at which to perform such a measurement. It can be seen from Table 3 that for a fixed latitude and date, such a θ_i value appears independent of water type (i.e., independent of ω). This solar zenith angle θ_i for zero inaccuracy, does however, exhibit a strong dependence on both geographic latitude

and Julian day. These dependencies are illustrated in Figure 4 wherein these θ_i values have been plotted against latitude of observation (degrees North) for the two equinoxes and two solstices. Obvious similarities exist between the equinoxial and winter curves. A distinct difference, however, is noted for the summer curve. This is a direct consequence of the tilt of the earth's axis to the plane of the ecliptic. This tilting results in a semiannual oscillation in the minimum solar zenith angle being observed at low latitudes. This is schematically illustrated in Figure 5 wherein the minimum solar zenith angle observable at intervals of 10°N latitude are plotted (in straight-line representation neglecting the sinusoidal nature of such variations) as a function of date throughout a solar year. Whereas the minimum solar zenith angle for March/September and December monotonically increases with increasing northern latitudes, the minimum solar zenith angle for June initially decreases until a latitude of 23½°N is reached, beyond which point it monotonically increases with increasing latitude. This explains the point of inflection occurring at 23½°N latitude in the June curve of Figure 4.

The last column in Table 3 lists the % inaccuracy in the determination of primary production when a k_v determined (at any θ_i) under totally overcast skies is applied to the primary production determinations for clear days. It is shown elsewhere (Jerome et al., 1982) that determining k_v under such overcast conditions is equivalent to determining k_v under clear sky conditions for a solar zenith angle of about 40° to 50°, and consequently the % inaccuracies

listed in the last column of Table 3 are comparable with the % inaccuracies listed in the 40° and 50° solar zenith angle columns.

The % inaccuracies listed in Table 3 are, in general, not large ($<\pm 15\%$) and, in most instances quite small ($<\pm 10\%$). Consequently, it is evident that a failure to consider the solar zenith angle dependence of the subsurface irradiance levels does not dramatically alter the total daily integrated value of primary production. However, if the irradiation (irradiance multiplied by incubation time) at a given depth in the water column is required for in situ incubation analysis, then a failure to consider the solar zenith angle dependence of the subsurface irradiance levels can significantly alter the estimate of irradiation, as shown below.

DETERMINATION OF SUBSURFACE IRRADIATION

Combining equations (5) and (6), the irradiance at a depth Z for a subsurface refracted angle θ_r and an incident radiation comprised of both a direct and a diffuse component may be written

$$E(Z,\theta_r) = E_o(\theta_r)\ (1-F)e^{-kZ/f(\theta)} + E_o(\theta_r)\ Fe^{-kZ/r} \qquad (13)$$

where each term is as previously defined.

The subsurface irradiation $\Gamma(Z)$ at depth Z for the entire day is obtained by integrating equation (13) over the daylight period.

$$\Gamma(Z) = 2 \int_{\theta_1}^{\theta_2} E(Z, \theta_r)\, d\theta_r$$

$$= 2 \int_{\theta_1}^{\theta_2} E_o(\theta_r) \left[(1-F)e^{-kZ/f(\theta)} + Fe^{-kZ/r}\right] d\theta_r \qquad (14)$$

where θ_1 = the subsurface refracted angle for the minimum solar zenith angle of the day considered, and

θ_2 = the subsurface refracted angle at sunrise or sunset (48.6° for water of index of refraction 4/3).

Solutions to equation (14) were found by performing an heuristic mental experiment.

It was assumed that an irradiance profile was taken at a given time (i.e., at a given value of θ_r) and the depths Z_x of the 30%, 10%, 3% and 1% irradiance levels were determined (i.e., for X = 0.30, 0.10, 0.03, 0.01). Irradiation calculations performed at these levels using a constant value of k_v would give values of 30%, 10%, 3% and 1%, respectively of the total daily irradiation just below

the surface of the water. Thus, it is these values of irradiation ($X\Gamma(0)$ where X is the irradiance level) that would be used for a sample incubated at these depths. These values of $X\Gamma(0)$ are labelled $\Gamma'(Z_x)$ and are taken as representative of the irradiation that would be estimated if the solar zenith angle dependence of subsurface irradiance levels were ignored.

It is now imagined that at these fixed depths Z_x *in situ* incubation is performed throughout the day (i.e., θ_Γ is varying). This is equivalent to remaining at a fixed depth, but not at a fixed subsurface irradiance level. A diurnal variation of the irradiance levels at these depths (Figure 2) would be observed as the levels migrate above and/or below the fixed depths Z_x. The daily integrated values of these varying irradiances would then yield the actual irradiation $\Gamma(Z_x)$ at the depth Z_x from equation (14).

The % inaccuracy in the determination of irradiation by neglecting the effects of solar zenith angle dependence on subsurface irradiance levels was then defined as

$$\% \text{ Inaccuracy} = \frac{\Gamma'(Z_x) - \Gamma(Z_x)}{\Gamma(Z_x)} \cdot 100\%$$

$$= \frac{X\Gamma(0) - \Gamma(Z_x)}{\Gamma(Z_x)} \cdot 100\% \qquad (15)$$

Equations (14) and (15) were solved, using half-hour averages, in a manner similar to the solving of equations (11) and (12). Various values of k were assumed, and once again the % inaccuracy was independent of the selection of k, but strongly dependent upon geographic latitude, Julian day, and water type.

DISCUSSION II

Figure 6 displays the % inaccuracies in the estimation of irradiation resulting from the assumption of a fixed depth for each of the 30%, 10%, 3%, and 1% irradiance levels for 0° latitude and the March/September equinoxes. These % inaccuracies are plotted as a function of the solar zenith angle at which the depths of the irradiance levels were determined. Figure 7 displays these % inaccuracies for 0° latitude and the June/December solstices. Both Figures 6 and 7 consider water types defined by ω = 0.60, 0.75, and 0.90. Figure 8 considers the % inaccuracy in the estimation of irradiation at a fixed latitude of 30°N for March and June for the 30% and 1% irradiance levels. Again all 3 water types are shown. Figure 9 considers the % inaccuracies associated with the 1% irradiance level at 30°N latitude for all 3 water types throughout the year.

A consideration of Figures 6 to 9 reveals that:

a) The % inaccuracies in irradiation determination increase with decreasing values of subsurface irradiance levels (Figures 6 and 7).

b) The % inaccuracies vary from a large overestimation of irradiation at small zenith angles to a large underestimation at large zenith angles, passing through a point of zero inaccuracy at some intermediate value of solar zenith angle θ_i (Figures 6, 7, 8, and 9).

c) Each assumed irradiance level has its own associated θ_i of zero inaccuracy (Figures 6, 7 and 8).

d) The magnitudes of the % inaccuracies decrease with increasing ω (Figure 8).

e) The θ_i associated with zero inaccuracy in the determination of irradiation is independent of ω (Figure 9).

f) The relative overestimation or underestimation of irradiation is a function of time of year and the difference between the solar zenith angle at which irradiance levels are determined and the solar zenith angle which results in a zero inaccuracy for a given irradiance level (Figure 9).

The relative overestimation or underestimation of irradiation is also a function of geographic latitude. This is illustrated in Figures 10(a) and 10(b) which show the % inaccuracy in irradiation determination (for a water mass of $\omega = 0.60$) plotted as a function of the solar zenith angle at which the depths of the 30% irradiance level (Figure 10(a)) and the 1% irradiance level (Figure 10(b)) were determined. Such % inaccuracies are shown for latitudes of 0°, 30°N, and 60°N during the equinox and solstice periods. The relative magnitudes of the % inaccuracies are clearly seen to be dependent upon the difference between the solar zenith angle at which irradiance levels are determined and the solar zenith angle which results in a zero inaccuracy for a given irradiance level. Therefore, to minimize inaccuracies in irradiation determinations, irradiance profiles should be taken at specific solar zenith angles which are dependent upon both latitude and date. This dependence of solar zenith angle for zero inaccuracy upon latitude and date is illustrated in Figure 11 for the 30% and 1% irradiance levels. The values for the 30% irradiance level are identical to the values in Figure 4.

SUMMARY

The effect of the solar zenith angle dependence of subsurface irradiance levels on the determination of daily primary production is small ($<15\%$) for any latitude and date.

However, this solar zenith angle dependence becomes significant when determining irradiation values for *in situ* incubations. If daily incubations are considered then irradiance profiles taken at the solar zenith angles given in Figure 11 provide the best measurements for calculating irradiation. For *in situ* incubations of shorter time periods, the k_v time dependence illustrated in Figure 3 can be effectively utilized to determine a solar zenith angle at which to estimate a suitable value of k_v.

REFERENCES

Davies, J.A., Schertzer, W. and Nunez, M. 1975. Estimating global radiation. Boundary-Layer Meteorol. 9:33-52.

Fee, E.J. 1969. A numerical model for the estimation of photosynthetic production, integrated over time and depth, in natural waters. Limnol. Oceanogr. 14:906-911.

Jerlov, N.G. 1976. Marine Optics. Elsevier, Amsterdam.

Jerome, J.H., Bruton, J.E. and Bukata, R.P. 1982. Influence of scattering phenomena on the solar zenith angle dependence of in-water irradiance levels. To appear in Appl. Opt.

Patten, B.C. 1968. Mathematical models of plankton production. Int. Rev. Gesamten Hydrobiol. 53:357-408.

Petzold, T.J. 1972. Volume scattering functions for selected waters. SIO Ref. 72-78, Scripps Institution of Oceanography, U. California at San Diego.

Smith, E.L. 1936. Photosynthesis in relation to light and carbon dioxide. Proc. Natl. Acad. Sci. U.S. 22:504.

Talling, J.F. 1957. The phytoplankton population as a compound photosynthetic system. New Phytologist 56:133-149.

Vollenweider, R.A. 1965. Calculation models of photosynthesis-depth curves and some implications regarding day rate estimates in primary production measurements. Mem. Ist. Ital. Idrobiol. 18 (Suppl):425-457.

FIGURE CAPTIONS

Figure 1. Ray diagram illustrating the passage of incident radiation into the water column

Figure 2. The relative depth of the 30%, 10%, 3% and 1% subsurface irradiance levels as a function of solar zenith angle
a) for a water mass defined by $\omega = 0.60$
b) for a water mass defined by $\omega = 0.90$

Figure 3. Solar zenith angle dependence of k_v for water masses defined by $\omega = 0.60$, $\omega = 0.75$ and $\omega = 0.90$

Figure 4. The solar zenith angle at the time of k_v determination for zero inaccuracy in the determination of daily primary production as a function of latitude of observation for different times of year

Figure 5. A straight-line representation of the minimum solar zenith angle observable in northern latitudes throughout the year

Figure 6. The percent inaccuracies in the estimation of irradiation for each of the 30%, 10%, 3% and 1% irradiance levels for 0° latitude and the March/September equinoxes

Figure 7. The percent inaccuracies in the estimation of irradiation for each of the 30%, 10%, 3% and 1% irradiance levels for 0° latitude and the June/December solatices

Figure 8. The percent inaccuracies in the estimation of irradiation for the 30% and 1% irradiance levels at 30°N latitude in March and June

Figure 9. The percent inaccuracies in the estimation of irradiation for the 1% irradiance levels at 30°N latitude for all three considered water types throughout the year.

Figure 10. The percent inaccuracy in the determination of irradiation for three latitudes

a) for the 30% irradiance level and a water mass defined by $\omega = 0.60$

b) for the 1% irradiance level and a water mass defined by $\omega = 0.60$

Figure 11. The solar zenith angle at the time of k_v determination for zero inaccuracy in the determination of irradiation as a function of latitude in June, March/September and December.

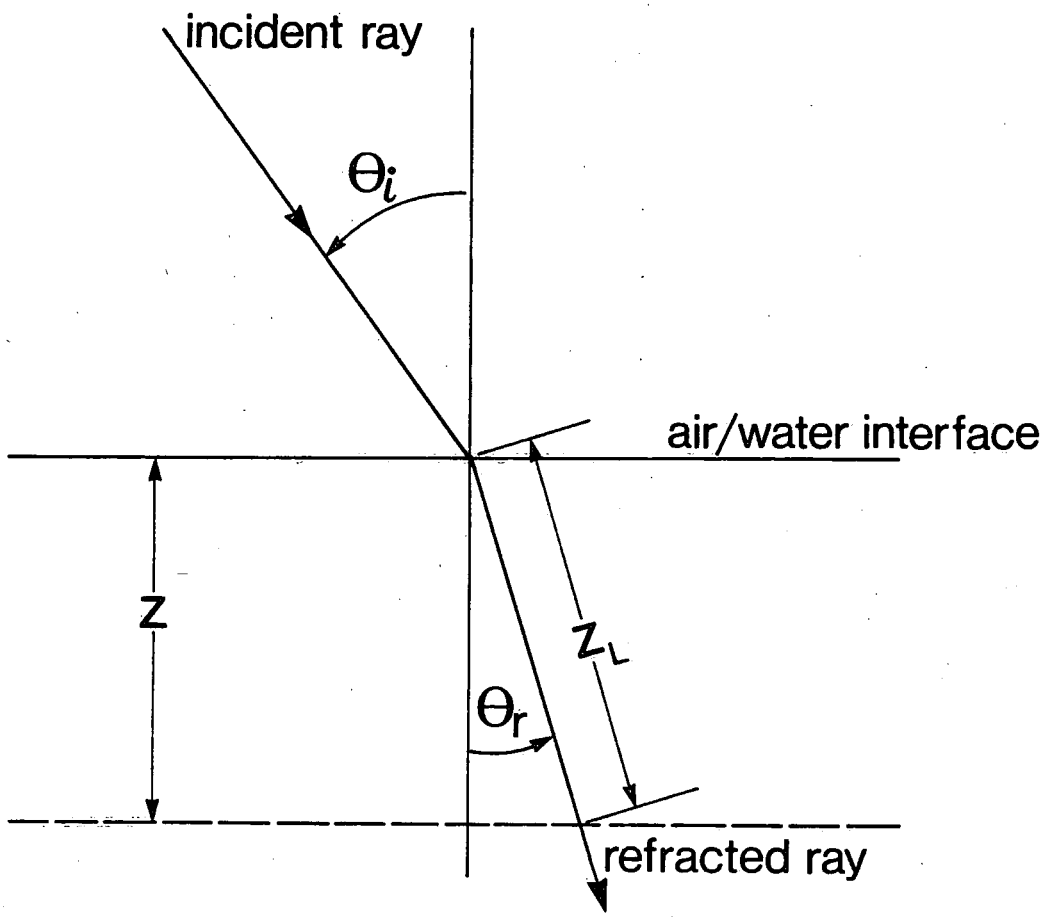
incident ray
θ_i
air/water interface
z
z_L
θ_r
refracted ray

FIG. 1

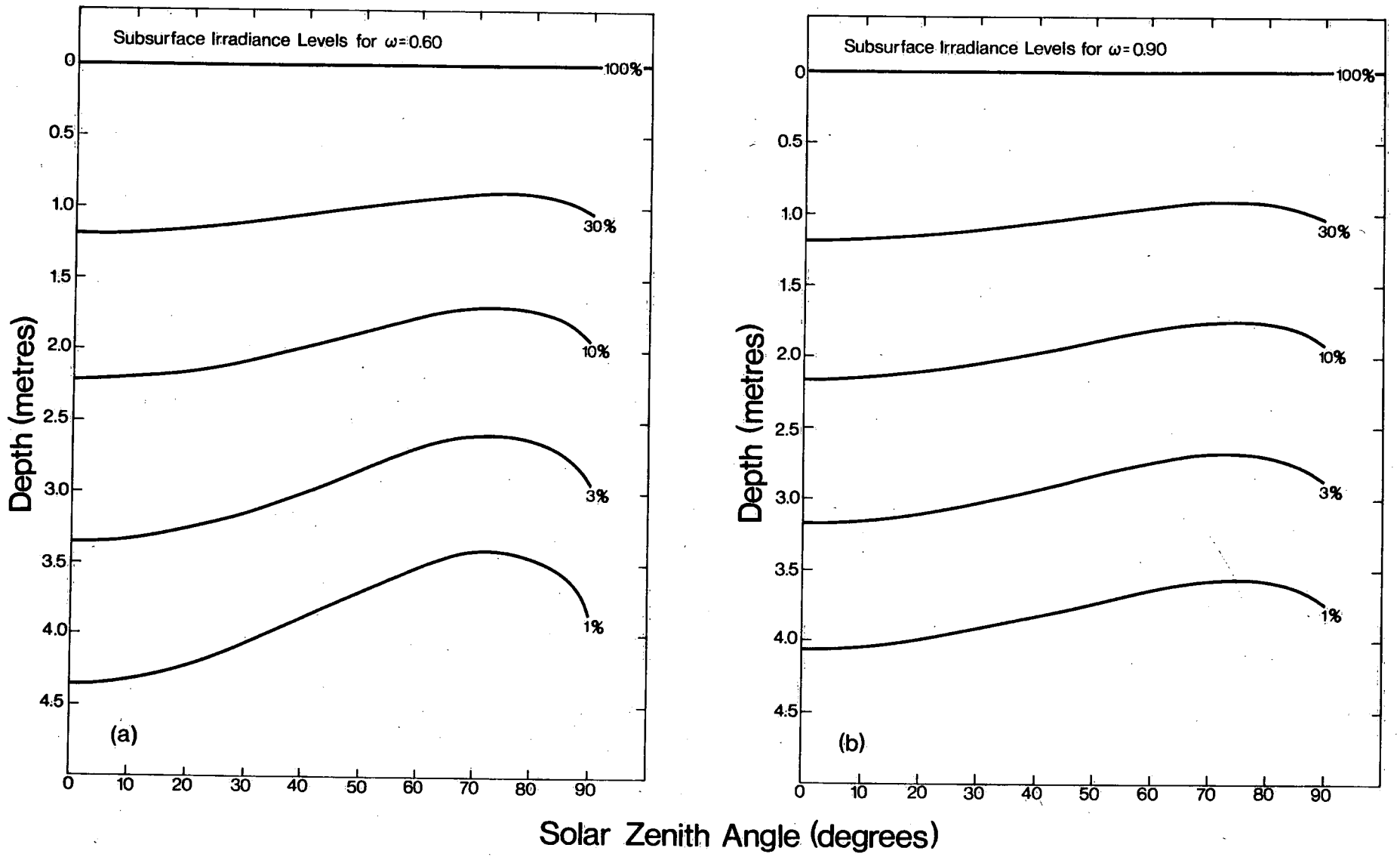
Subsurface Irradiance Levels for ω=0.60
Subsurface Irradiance Levels for ω=0.90
100%
30%
10%
3%
1%
Depth (metres)
0
0.5
1.0
1.5
2.0
2.5
3.0
3.5
4.0
4.5
(a)
(b)
0
10
20
30
40
50
60
70
80
90
Solar Zenith Angle (degrees)

FIG 2

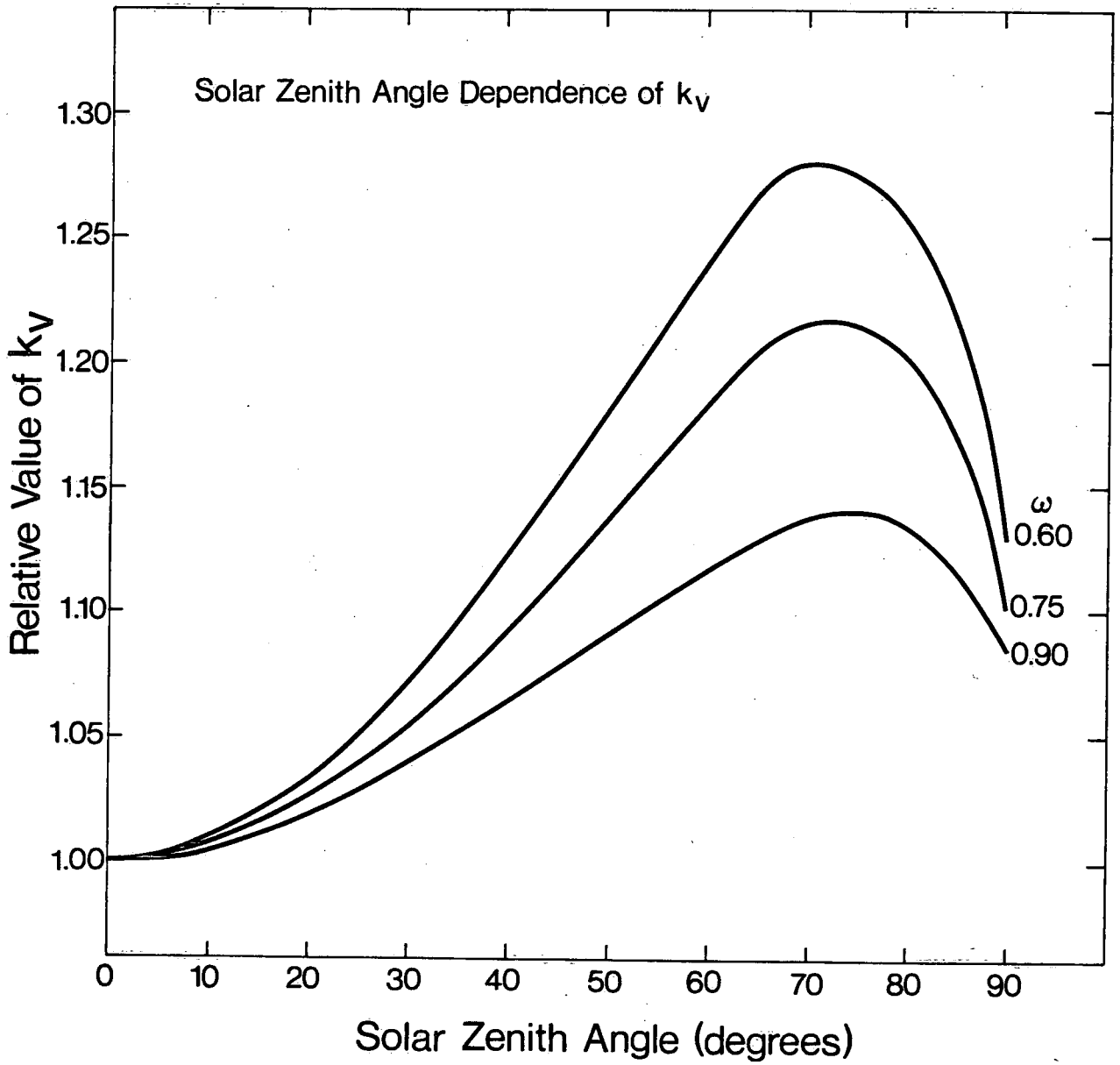
Solar Zenith Angle Dependence of k_V
Relative Value of k_V
1.30
1.25
1.20
1.15
1.10
1.05
1.00
0
10
20
30
40
50
60
70
80
90
Solar Zenith Angle (degrees)
ε
0.60
0.75
0.90

FIG 3

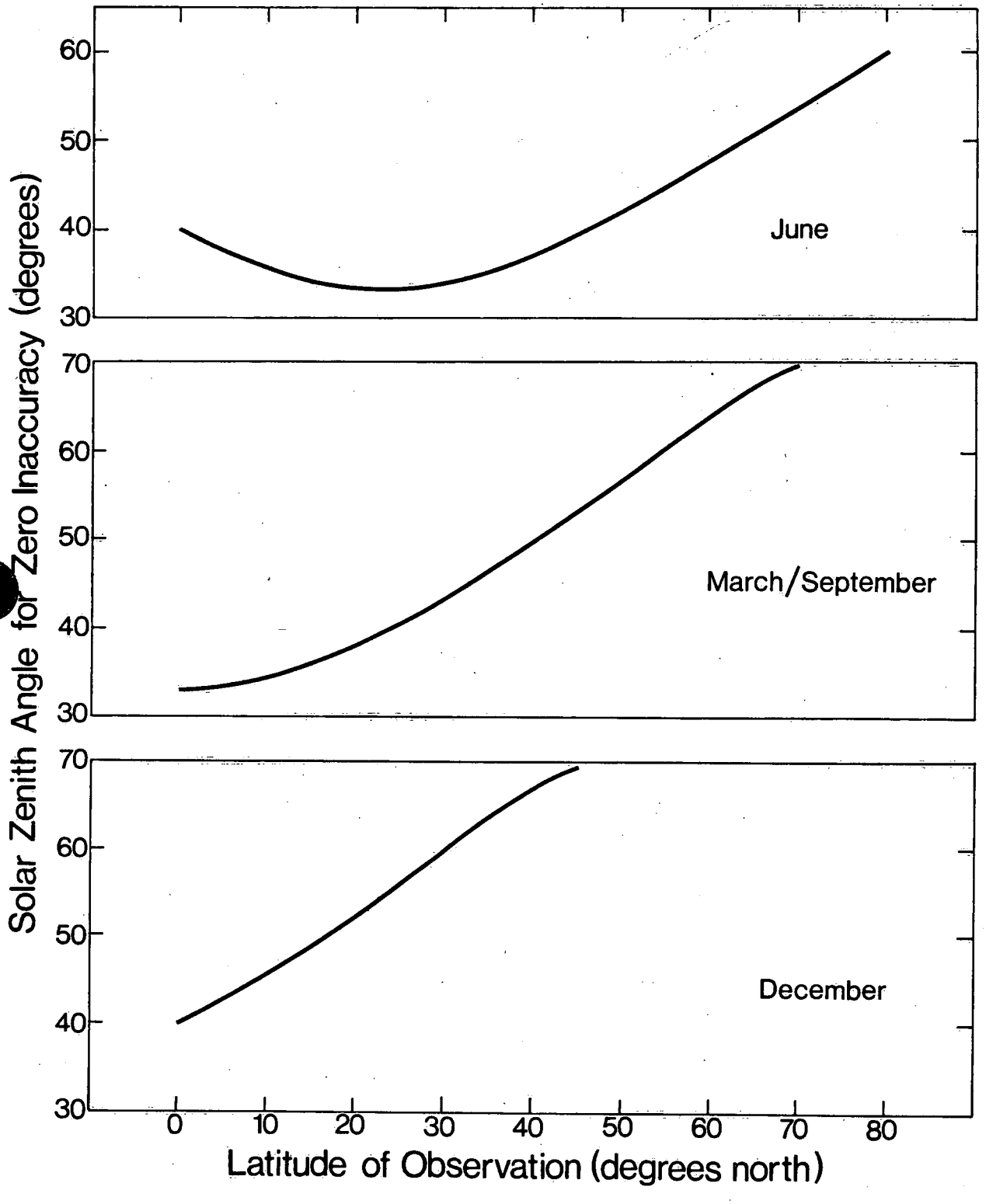
Solar Zenith Angle for Zero Inaccuracy (degrees)
60
50
40
30
June
70
60
50
40
30
March/September
70
60
50
40
30
December
0
10
20
30
40
50
60
70
80
Latitude of Observation (degrees north)

FIG 4

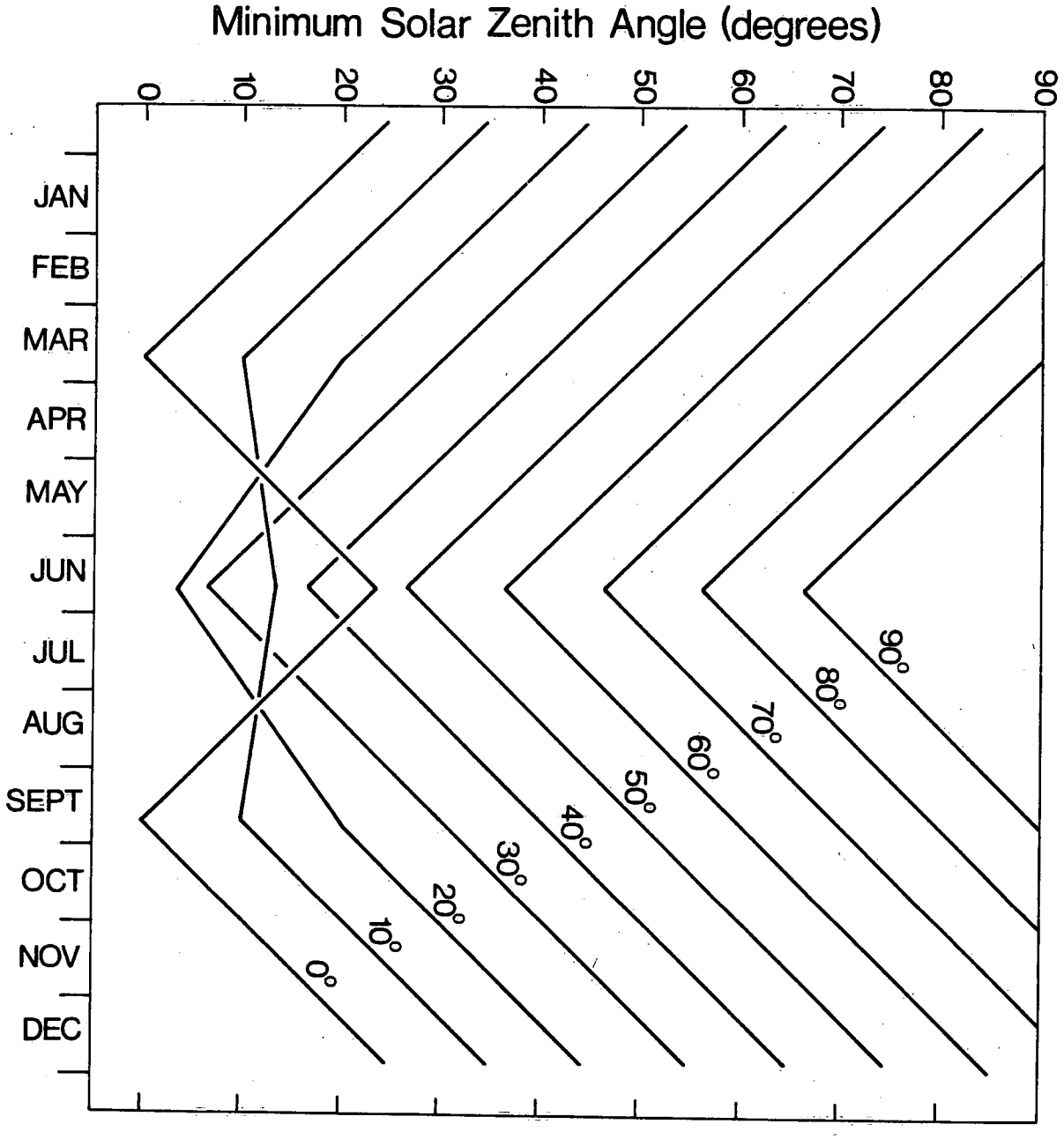
Minimum Solar Zenith Angle (degrees)
0
10
20
30
40
50
60
70
80
90
JAN
FEB
MAR
APR
MAY
JUN
JUL
AUG
SEPT
OCT
NOV
DEC
0°
10°
20°
30°
40°
50°
60°
70°
80°
90°

FIG 5

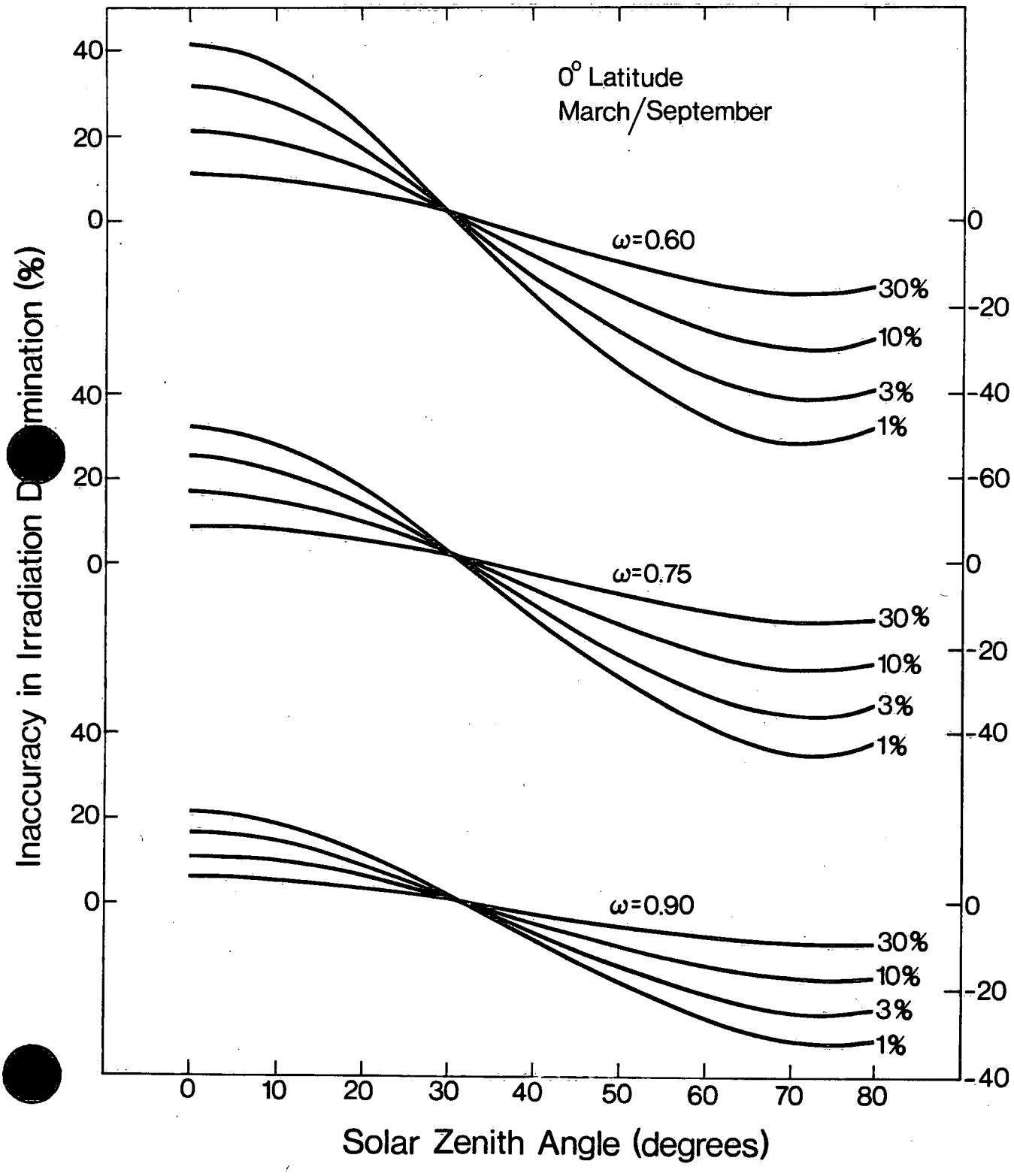
0° Latitude
March/September
ω=0.60
30%
10%
3%
1%
ω=0.75
30%
10%
3%
1%
ω=0.90
30%
10%
3%
1%
40
20
0
40
20
0
40
20
0
0
-20
-40
-60
0
-20
-40
0
-20
-40
0
10
20
30
40
50
60
70
80
Solar Zenith Angle (degrees)
Inaccuracy in Irradiation D mination (%)

FIG 6

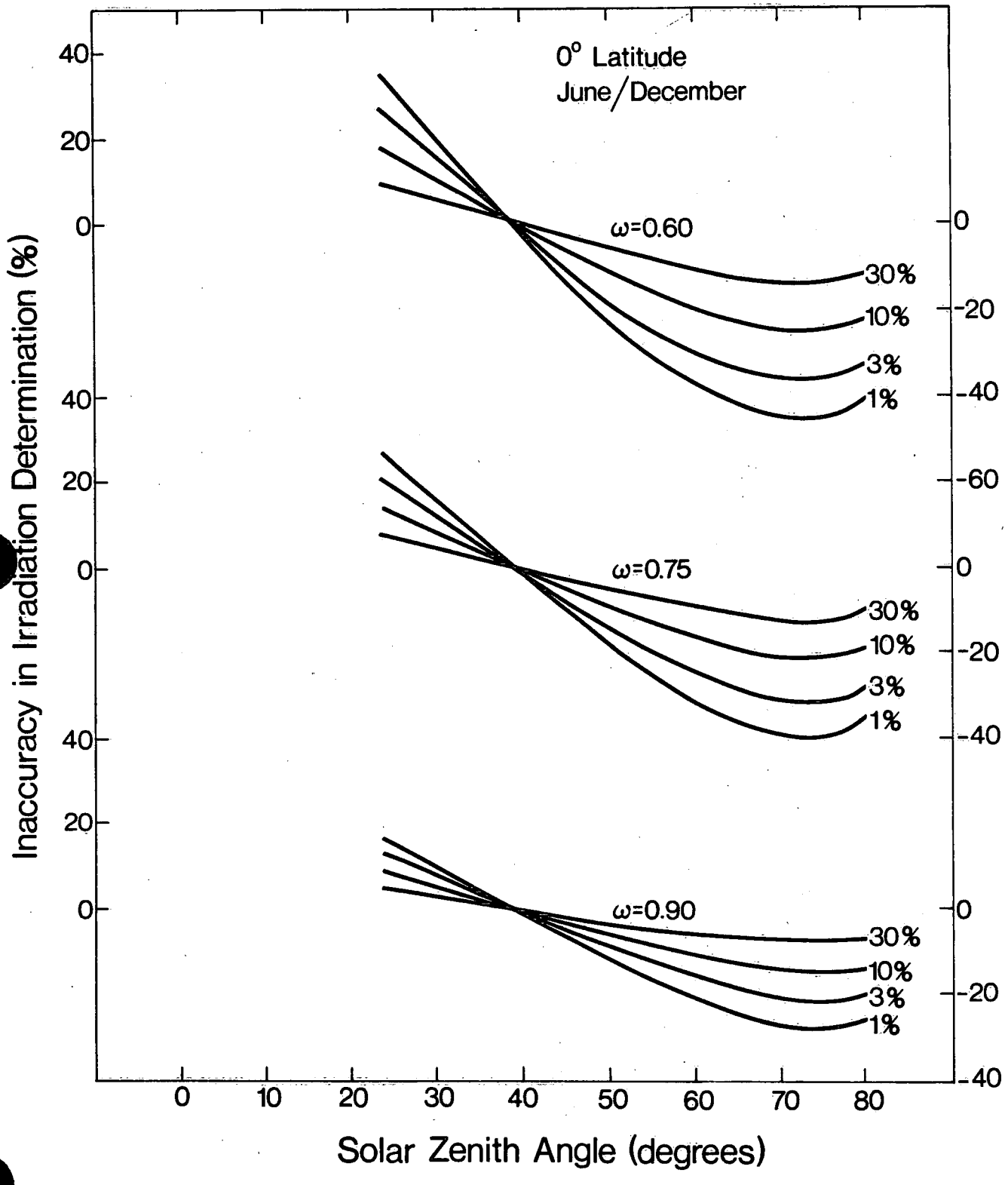
0° Latitude
June/December
ω=0.60
30%
10%
3%
1%
ω=0.75
30%
10%
3%
1%
ω=0.90
30%
10%
3%
1%
40
20
0
40
20
0
40
20
0
0
-20
-40
-60
0
-20
-40
0
-20
-40
0
10
20
30
40
50
60
70
80
Inaccuracy in Irradiation Determination (%)
Solar Zenith Angle (degrees)

FIG 7

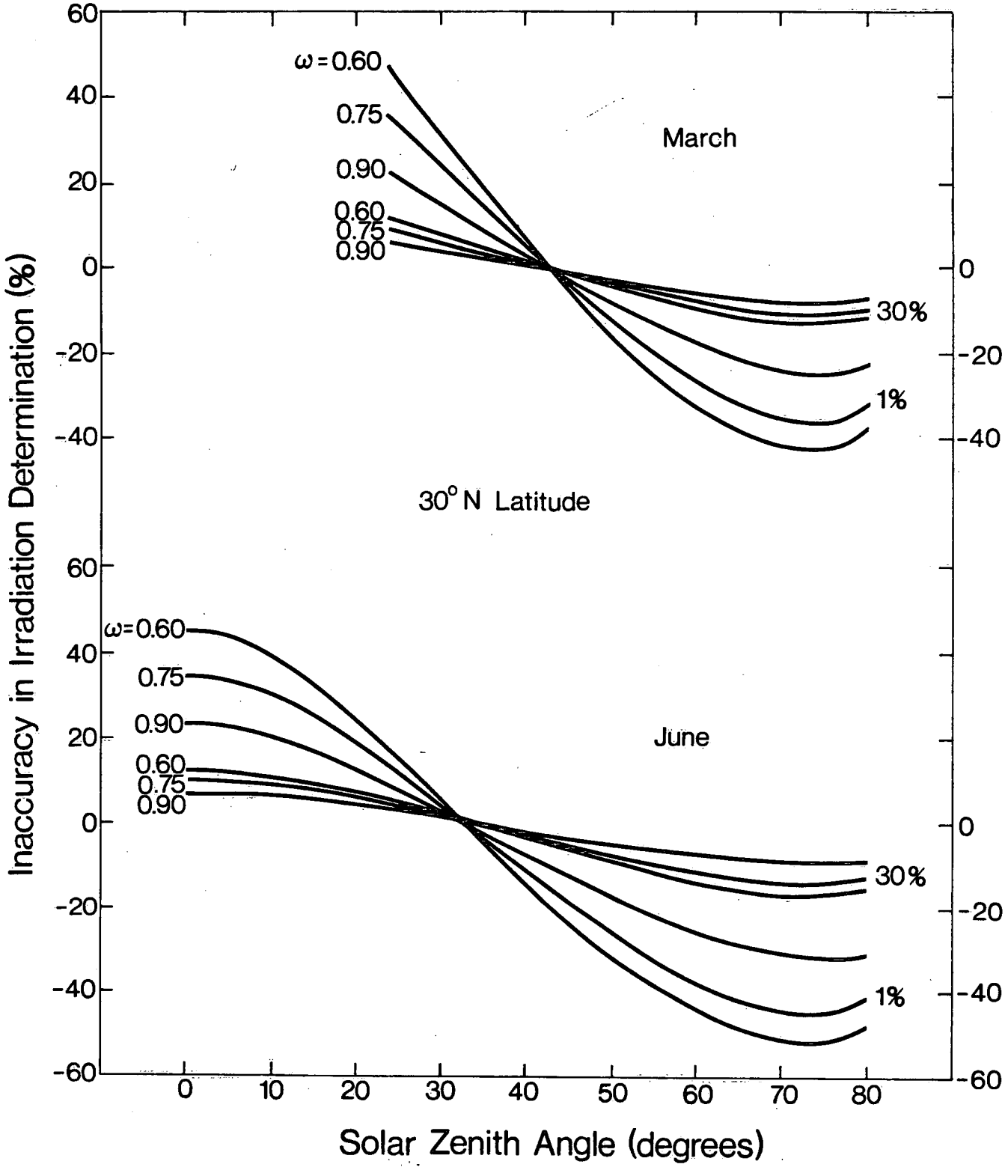
ω = 0.60
0.75
0.90
March
0.60
0.75
0.90
30%
1%
30° N Latitude
ω=0.60
0.75
0.90
June
0.60
0.75
0.90
30%
1%
Inaccuracy in Irradiation Determination (%)
Solar Zenith Angle (degrees)
60
40
20
0
-20
-40
-60
0
10
20
30
40
50
60
70
80

FIG 8

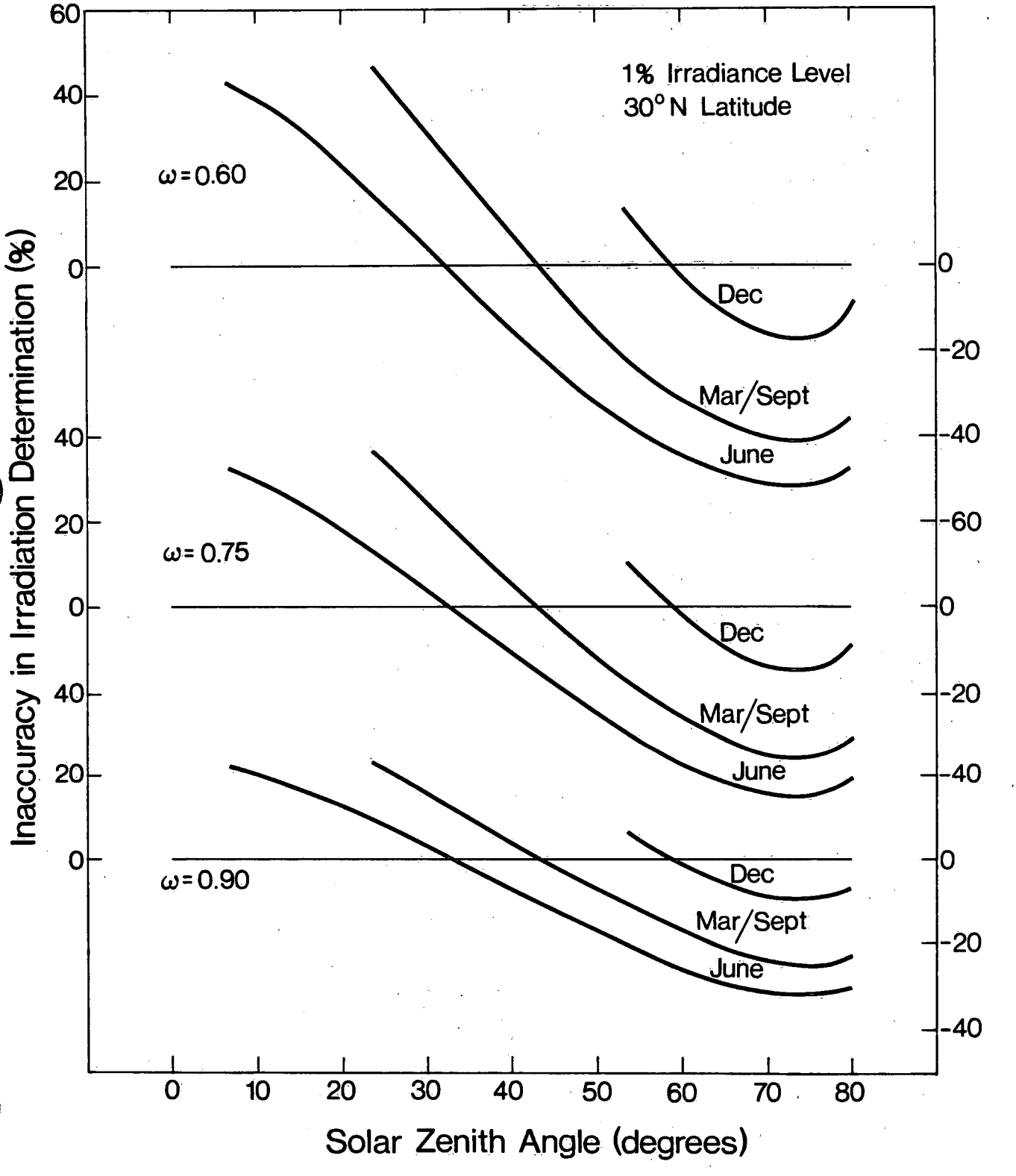
1% Irradiance Level
30° N Latitude
ω = 0.60
ω = 0.75
ω = 0.90
Dec
Mar/Sept
June
Inaccuracy in Irradiation Determination (%)
Solar Zenith Angle (degrees)
60
40
20
0
-20
-40
-60
0
10
20
30
40
50
60
70
80

FIG 9

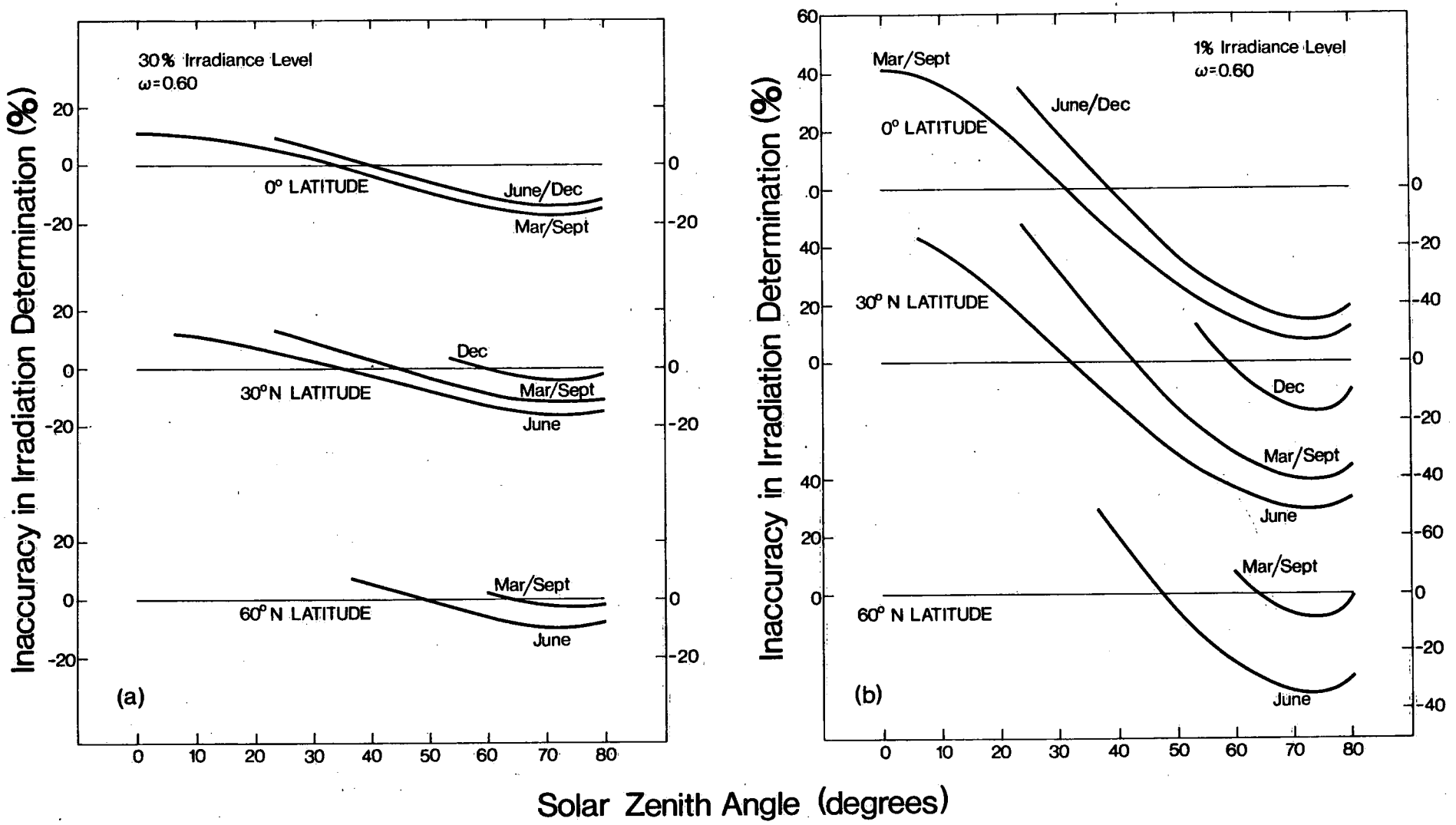
30% Irradiance Level
ω=0.60
0° LATITUDE
June/Dec
Mar/Sept
30°N LATITUDE
Dec
Mar/Sept
June
60° N LATITUDE
Mar/Sept
June
(a)
1% Irradiance Level
ω=0.60
Mar/Sept
June/Dec
0° LATITUDE
30° N LATITUDE
Dec
Mar/Sept
June
60° N LATITUDE
Mar/Sept
June
(b)
Inaccuracy in Irradiation Determination (%)
Solar Zenith Angle (degrees)

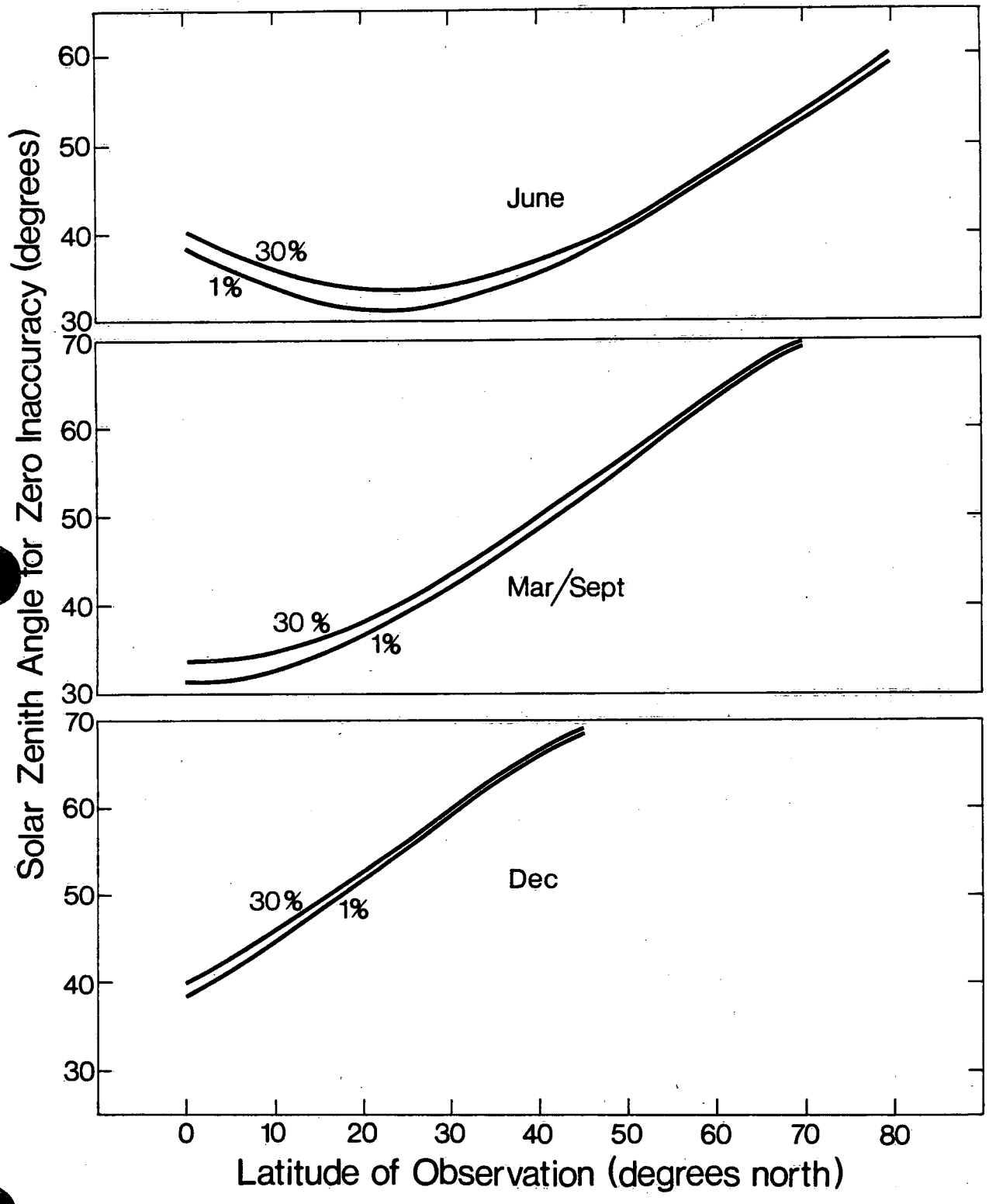
Solar Zenith Angle for Zero Inaccuracy (degrees)
60
50
40
30
June
30%
1%
70
60
50
40
30
Mar/Sept
30 %
1%
70
60
50
40
30
Dec
30%
1%
0
10
20
30
40
50
60
70
80
Latitude of Observation (degrees north)

FIG 11

TABLE CAPTIONS

Table 1. Incident radiation distribution as a function of solar zenith angle.

Table 2. Coefficients of series expansion.

Table 3. Percent inaccuracies in the estimation of daily primary production.

Table 1. Incident Radiation Distribution

Solar Zenith Angle (degrees)	Diffuse Component of Incident Radiation (per cent)
0	8.0
10	8.1
20	8.4
30	9.0
40	10.0
50	11.6
60	14.7
70	21.6
80	43.9
90	100.0

Table 2. Coefficients of Series Expansion

Subsurface Irradiance Level	Incident Radiation			
	Totally Direct			Totally Diffuse
	$r_1(\omega)$	$r_2(\omega)$	$r_3(\omega)$	r
30%				
$\omega = 0.60$	1.0	0.0	0.0	0.845
$\omega = 0.75$	1.0	0.0	0.0	0.848
$\omega = 0.90$	1.222	-0.412	0.190	0.853
10%				
$\omega = 0.60$	1.102	-0.169	0.067	0.858
$\omega = 0.75$	1.349	-0.671	0.322	0.866
$\omega = 0.90$	1.620	-1.015	0.395	0.881
3%				
$\omega = 0.60$	1.323	-0.612	0.289	0.867
$\omega = 0.75$	1.510	-0.845	0.335	0.879
$\omega = 0.90$	2.074	-1.831	0.757	0.899
1%				
$\omega = 0.60$	1.603	-1.213	0.610	0.877
$\omega = 0.75$	1.809	-1.389	0.580	0.901
$\omega = 0.90$	2.508	-2.597	1.089	0.914

Table 3. % Inaccuracies in Estimating Daily Primary Production

Latitude and Date	Solar Zenith Angle at Time of k_v Determination									Totally Diffuse
	0°	10°	20°	30°	40°	50°	60°	70°	80°	
0°										
March/September										
ω = 0.60	8	7	5	1	-3	-8	-12	-14	-13	-4
ω = 0.75	6	6	4	1	-2	-6	-9	-12	-11	-3
ω = 0.90	4	4	3	1	-2	-4	-6	-8	-7	-4
June/December										
ω = 0.60			8	4	0	-5	-9	-12	-10	-1
ω = 0.75			6	3	0	-4	-7	-10	-9	-1
ω = 0.90			4	2	0	-3	-5	-6	-6	-2
30°N										
March/September										
ω = 0.60			10	6	2	-3	-8	-10	-9	1
ω = 0.75			8	5	1	-3	-6	-9	-8	0
ω = 0.90			5	3	1	-2	-4	-5	-5	-1
June										
ω = 0.60	9	8	5	2	-3	-7	-11	-14	-13	-3
ω = 0.75	7	6	4	1	-2	-6	-9	-11	-10	-3
ω = 0.90	5	4	3	1	-1	-4	-6	-7	-7	-3
December										
ω = 0.60						4	0	-4	-2	9
ω = 0.75						4	0	-3	-2	7
ω = 0.90						2	0	-2	-2	3
60°N										
March/September										
ω = 0.60						6	1	-2	0	11
ω = 0.75						5	1	-1	1	8
ω = 0.90						3	1	-1	-1	4
June										
ω = 0.60				9	4	-1	-6	-8	-7	3
ω = 0.75				7	3	-1	-4	-7	-6	2
ω = 0.90				4	2	0	-3	-4	-4	0
December										
ω = 0.60									-5	6
ω = 0.75									-4	5
ω = 0.90									-2	2